OPEN ACCESS
JOURNAL OF ADVANCED DIELECTRICS
Vol. 11, No. 3 (2021) 2140002 (8 pages)

DOI: 10.1142/S2010135X21400026

Influence of the sintering temperature on ferroelectric properties of potassium-sodium niobate piezoelectric ceramics

J. A. Cortés[*], J. Camargo[†,¶], M. F. Rachia[*], F. Rubio-Marcos[‡,§]
L. Ramajo[†], M. Castro[†] and M. A. Ramírez[*]

[*]*Sao Paulo State University — UNESP*
Faculty of Engineering of Guaratingueta. Av.
Dr. Ariberto Pereira da Cunha 333, Portal das Colinas
12516-410, Guaratingueta, SP, Brazil

[†]*Research Institute for Materials Science and Technology*
INTEMA, Av. Colon 10850, B7608FDQ
Mar del Plata, Argentina

[‡]*Electroceramics Department, Instituto de Cerámica y Vidrio*
CSIC, Kelsen 5, 28049, Madrid, Spain

[§]*Escuela Politécnica Superior. Universidad Antonio de Nebrija*
Pirineos 55, 28040, Madrid, Spain

¶jcamargo@fi.mdp.edu.ar

Received 12 February 2021; Revised 17 March 2021; Accepted 31 March 2021; Published 23 April 2021

The effect of sintering condition on structure, microstructure, and ferroelectric properties of $(K_{0.44}Na_{0.52}Li_{0.04})(Nb_{0.86}Ta_{0.10}Sb_{0.04})O_3$ (KNL–NTS) has been investigated. Ceramic powders have been synthesized by the solid-state reaction method and sintered at different temperatures (1115 °C, 1125 °C, and 1140 °C). Then, samples were characterized by thermogravimetric analysis, X-ray diffraction, scanning electron microscopy, and impedance spectroscopy. Through XRD results, the perovskite structure and small peaks corresponding to a secondary phase were detected. Ceramics processed at the highest temperatures showed higher densities and good piezoelectric properties (d_{33}, K_p, and K_t), particularly specimens sintered at 1125 °C presented the highest piezoelectric performance.

Keywords: KNL–NTS; lead-free; ferroelectric properties.

1. Introduction

Lead zirconate-titanate piezoceramics are the most important and widely used materials for piezoelectric transducers, transformers, and sensors. These ceramics have played a dominant role in the piezoelectric field for a long time because of their excellent piezoelectric properties.[1–3] However, the toxicity due to the presence of more than 60% lead in the composition is a serious threat to human health and the environment. Consequently, lead-free piezoelectric ceramics have attracted great attention recently.[4–6]

Numerous studies have focused on the development of new piezoelectric harmless to the environment.[7–9] Compositions based on sodium-potassium niobate $K_xNa_{1-x}NbO_3$ (KNN), obtained by solution-based powder synthesis routes, such as the sol–gel and microemulsion mediated methods, have shown good properties.[10–12] Nevertheless, the use of soft-chemical methods cannot prevent the appearance of carbonates during the thermal process and requires high processing temperatures to sinter the obtained powders appropriately. Furthermore, the low piezoelectric coefficients (45 to 80 pC/N) registered,[13,14] impulse the development of new materials with improved properties.[15–17]

Saito *et al.* reported exceptionally high piezoelectric properties in $(K,Na)NbO_3$–$LiTaO_3$–$LiSbO_3$ piezoceramics,[17–20] through chemical modifications, in the vicinity of the morphotropic phase boundary (MPB) of KNN, by complex simultaneous substitutions in the A (Li) and B (Ta and Sb) sites of the perovskite lattice. KNN-based ceramic with 4 mol% of Li, 10 mol% of Ta, and 4 mol% of Sb was synthesized by the solid-state reaction method producing nanopowders with good sinterability that reach interesting piezoelectric properties.[21] The increase of alkaline elements on KNN reduces the solid-state reaction temperature, while it also reduces the densification and favors the reaction of the material with the moisture in the air showing deliquescence. Moreover, alkaline metal elements included in these materials easily evaporate at

¶Corresponding author.

high temperatures and the selective evaporation of constituents causes compositional fluctuations that result in the detriment of the material properties.[22] Also, the evaporation of alkaline elements during the sintering process can produce the presence of secondary phases, which affect the final ferroelectric properties.[5,18,23] Accordingly, it is significant to investigate the influence of the sintering temperature on the phases' evolution and its influence on the final properties.

In this manuscript, the sintering temperature effect on $(K_{0.44}Na_{0.52}Li_{0.04})(Nb_{0.86}Ta_{0.1}Sb_{0.04})O_3$ ceramics (KNL–NTS), obtained by the solid-state reaction method, is reported. Experimental results were discussed considering the effect of the sintering temperature on the stabilized structure, and the final microstructural, dielectric, and piezoelectric properties. Specifically, these results demonstrate that sintering conditions play a relevant role in the functional properties of the potassium-sodium niobate-based lead-free piezoceramics.

2. Experimental Procedure

Ceramic powders with nominal $(K_{0.44}Na_{0.52}Li_{0.04})$-$(Nb_{0.86}Ta_{0.1}Sb_{0.04})O_3$ (KNL–NTS) composition were synthesized by the solid-state reaction route. Na_2CO_3, Li_2CO_3 (Panreac, 99.5%), K_2CO_3 (Merck, 99%), Nb_2O_5, Ta_2O_5, and Sb_2O_5 (Sigma–Aldrich, ≥ 99.5%, 99.9%, 99%, and 99.995%, respectively) were used as starting raw materials. They were individually milled to obtain an appropriate particle size distribution. Powders were mixed and milled in an isopropyl alcohol medium in a laboratory ball mill with zirconia balls for 24 h. The resulting powders were dried at 110 °C and passed through a sieve of 200 mesh. The calcined temperatures were obtained employing a TG-DTA equipment (Netzsch, STA 409 model) from 20 °C to 1000 °C with a 10 °C/min heating rate in a static atmosphere. Afterward, powders were calcined at 750 °C for 2 h at 3 °C/min. The calcined powders were milled again in the ball mill and pressed at 200 MPa into disks of 12 mm in diameter and 1.2 mm thick. The disks were finally sintered in air at 1115 °C, 1125 °C, or 1140 °C for 2 h in an electric furnace using air atmosphere.

Crystalline phases were characterized by X-ray diffraction patterns on the calcined powder and sintered disks using an X-Ray diffractometer (Bruker D8 Advance Eco) operating at 40 kV/25 mA with a CuKα radiation source (λ = 1.5404 Å), with a monochromator, in the range of 20° to 80°, with incremental steps of 0.02°. The crystalline phases were identified based on the Inorganic Crystal Structure Database (ICSD). The phases' percentages were determined from the area under the peaks corresponding to each phase. The samples were polished and thermally etched and analyzed using a Scanning Electron Microscope (SEM ZEIS model EBO LS-15). The specific gravity was obtained by a standard test method for water absorption (ASTM C373-14a).

For the electrical measurements, a fired silver paste was used for the electric contacts. The samples were polled in a silicon oil bath at 25 °C by applying a DC field of 3 kV/mm for 30 min. The piezoelectric constant d_{33} was measured using a piezo d_{33} meter (YE2730A d_{33} METER, APC International, Ltd., USA). Dielectric properties were determined at different temperatures and frequencies using an impedance analyzer HP4284A in the frequency range 100 Hz–1 MHz, while the ferroelectric nature of the ceramics was determined using a hysteresis meter (RT 6000 HVS, RADIANT Technologies). Finally, the planar coupling coefficient (K_p) and electromechanical coupling factor (K_t) were calculated employing an impedance analyzer espace, Hioki 3535, and using Eqs. (1) and (2), respectively.[18]

$$K_p = \left[2.51\left(\frac{f_p - f_s}{f_s}\right)\right]^{\frac{1}{2}}, \tag{1}$$

$$K_t = \left[\frac{\pi}{2}\frac{f_p}{f_s}\tan\frac{\pi}{2}\frac{f_p - f_s}{f_p}\right]^{\frac{1}{2}}, \tag{2}$$

where f_s is defined as the frequency of maximum conductance and f_p is defined as the frequency of maximum resistance.[24]

3. Results and Discussion

Figure 1 shows the TGA curve corresponding to KNL–NTS raw mixture obtained by the solid-state reaction route. To determine the temperature at which each mass loss occurs, the derivative of the mass loss curve is used and shown in Fig. 1. Then, it is possible to observe ~13% overall weight loss from RT to 1000 °C. TGA figure has two main weight

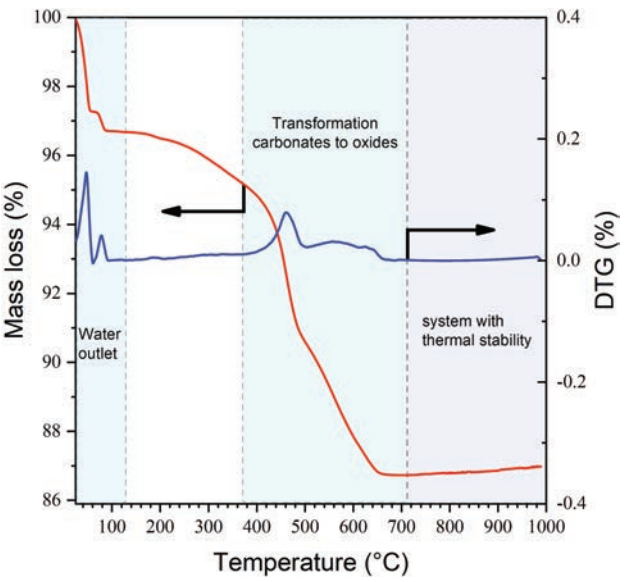

Fig. 1. Thermogravimetric analysis of the KNL–NTS raw mixture.

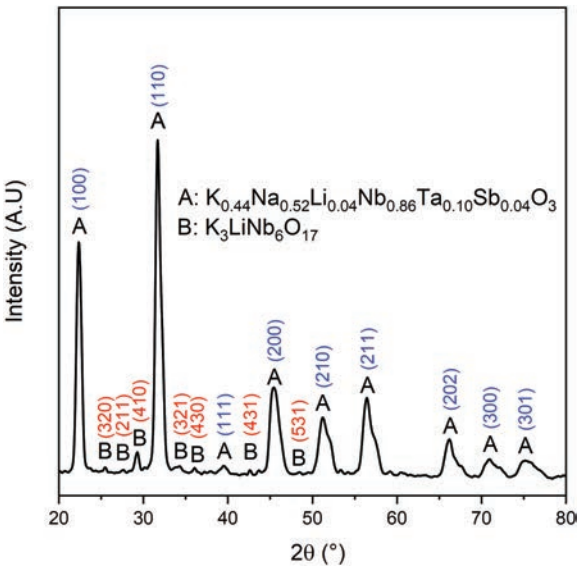

Fig. 2. XRD patterns corresponding to the KNL–NTS powder calcined at 750 °C for 2 h.

loss zones, the first one of ~3% in temperature range between RT and 120 °C can be related to vaporization of water, while the second one of ~8% in temperature range between 400 °C and 670 °C can be associated to the carbonates' decomposition for the final reaction. Finally, the absence of significant mass loss changes at temperatures above 650 °C indicates that the thermodynamic stability is reached. Based on these results, the selected heat treatment was carried out at 750 °C for 2 h in a muffle furnace using air atmosphere, to guarantee the complete decomposition of the carbonates of the A-elements and the formation of the perovskite phase.

Figure 2 presents the X-ray diffraction pattern of the KNL–NTS powder calcined at 750 °C for 2 h. This pattern reveals the presence of the KNL–NTS phase and a little amount of the $K_3LiNb_6O_{17}$ (KLNO) secondary phase with tetragonal tungsten-bronze phase structure (TTB) and P4/mbm space group.[25–27] This secondary phase is associated with possible inhomogeneities in the B-site of the perovskite, as was related by Ramajo *et al.*[18] Additionally, the alkali metals evaporation, during the thermal treatment, could produce A-site vacancies inducing the stabilization of a nonstoichiometric perovskite.

Figure 3 shows three principal peaks of the KNL–NTS powder, corresponding to 22.5°, 31.5°, and 45.5° Bragg angles. The peaks near 22.5° and 45.5° show the tetragonal and orthorhombic phases stabilization, whereas the principal peak near 31.5° only registers the tetragonal contribution. These results suggest that the MPB composition is reached in the synthesized powder.

Figure 4 displays the X-ray diffraction patterns of sintered ceramics at 1115 °C, 1125 °C, and 1140 °C for 2 h. It is possible to observe the stabilization of the perovskite phase and the remaining secondary phase. Besides, Table 1

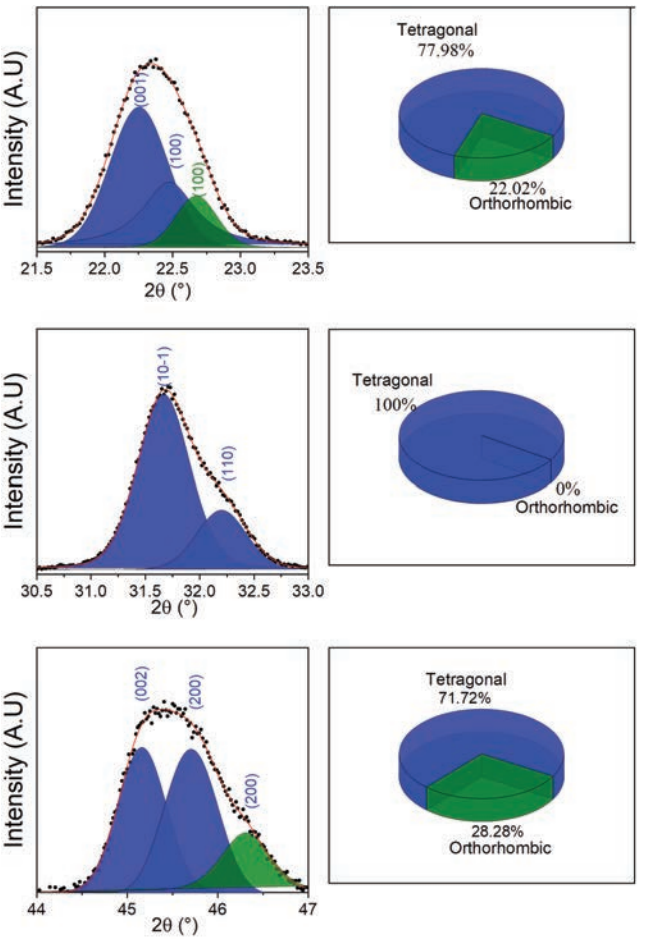

Fig. 3. Principal XRD peaks corresponding to the KNL–NTS powder calcined at 750 °C for 2 h with the respective tetragonal and orthorhombic contributions.

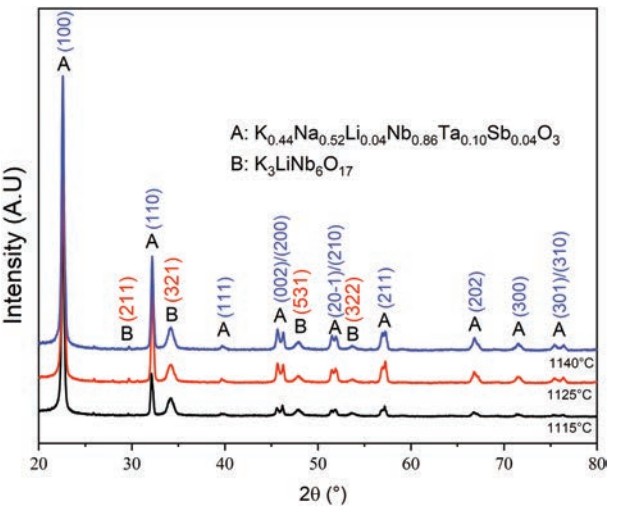

Fig. 4. XRD patterns corresponding to KNL–NTS ceramics sintered at 1115 °C, 1125 °C, and 1140 °C for 2 h.

Table 1. Principal XRD peaks corresponding to the KNL–NTS powder calcined at 750 °C for 2 h and sintered at 1115 °C, 1125 °C, and 1140 °C, with the respective tetragonal (T) and orthorhombic (O) contributions.

Sample	(100) ~22.5°		(110) ~31.5°		(200) ~45.5°	
	T	O	T	O	T	O
750°C	77.98	22.02	100	0	71.72	28.28
1115°C	37.26	62.74	100	0	53.55	46.45
1125°C	41.06	58.94	100	0	57.37	42.62
1140°C	37.50	62.50	100	0	60.27	39.73

Table 2. KLNO amount percentage from XRD patterns corresponding to the KNL–NTS disks sintered at 1115 °C, 1125 °C, and 1140 °C.

Sample	750 °C	1115 °C	1125 °C	1140 °C
KLNO (%)	12.5	11.3	9.5	10.0

shows the proportion of tetragonal and orthorhombic peaks in the sintered samples and the calcined powder. From the table, it can be observed an increase in the KNL–NTS orthorhombic proportion on the sintered samples. Furthermore, from Figs. 2 and 4, the (100) peak is turned in the principal peak in the sintered ceramics while the peak assigned only to the tetragonal phase ((110) plane) decreases. This behavior confirms the stabilization of the MPB and a displacement in the orthorhombic/tetragonal ratio in the sintered samples.

Additionally, considering the KLNO amount from the XRD patterns detailed in Table 2, it can be observed that the secondary phase amount is sensitive to the sintering temperature. Indeed, the KLNO phase amount diminishes for the samples sintered at 1125 °C while it increases for higher temperatures. This secondary phase retains part of the elements modifying the perovskite composition. During the sintering treatment, the diffusion of the ions diminishes the KLNO formation. However, for the highest temperatures, the volatilization of the alkaline elements[25] and the increasing grain size could favor the secondary phase formation.

The microstructural evolution and the grain size distribution (GSD) of KNL–NTS ceramics as a function of sintering temperature are shown in Fig. 5. It can be observed, in samples sintered at 1115 °C and 1125 °C, small porosity traces, which diminishes in ceramics obtained at the highest temperature. In all cases, specimens show typical morphology of well-defined polyhedral grains. Taking into account the GSDs, it is possible to observe that the average grain size increases from 0.73 ± 0.43 μm (1115 °C) to 0.97 ± 0.55 μm (1140 °C). The pictures also reveal a wide GSD, where the small grains' fraction prevails. It is known that the densification of KNL–NTS ceramics proceeds through the formation of a liquid phase.[25] This liquid phase favors the atomic

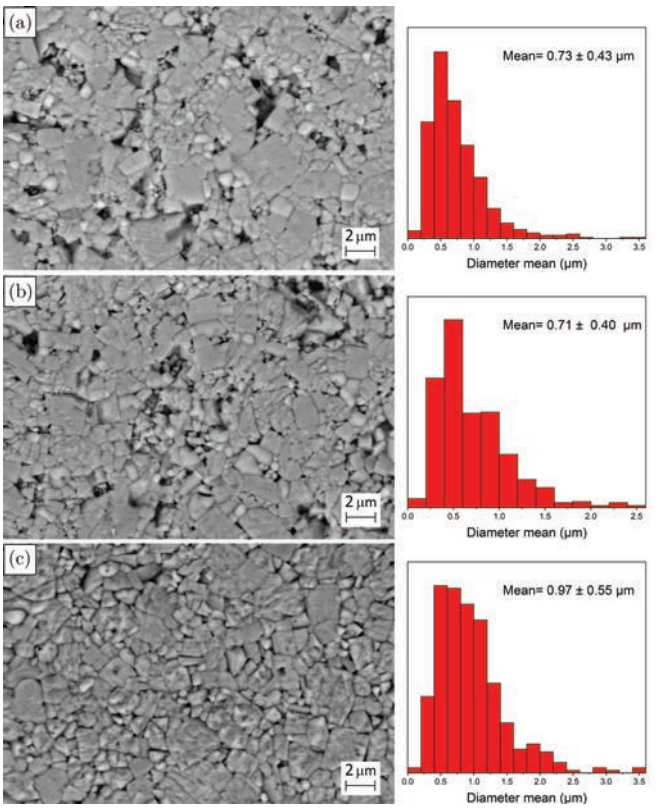

Fig. 5. SEM images of KNL–NTS sintered at (a) 1115 °C, (b) 1125 °C and (c) 1140 °C. The grain size distribution is plotted to the right each SEM image.

Table 3. Density (ρ), piezoelectric constant (d_{33}), planar coupling coefficient (K_p), and electromechanical coupling factor (K_t) of KNL–NTS sintered ceramics.

Sample KNL–NTS	ρ (%)	d_{33} (pC/cm)	K_p (%)	K_t (%)
1115 °C	93	145	24.2	38.6
1125 °C	93	190	29.1	39.3
1140 °C	95	170	23.8	26.8

mobility and, consequently, facilitates and accelerates the kinetics of the sintering process. Moreover, the volatilization of the alkali elements during sintering induces an excess of B-site ions and the appearance of the liquid phase. In addition, the secondary phase formation can also influence the grain growth due to the partial retention of the elements of the main phase and to the possible pinning effect to grain boundaries.

Densities of the sintered samples are reported in Table 3. Although all the samples registered high-density values, the samples sintered at 1140 °C exhibited the highest densification

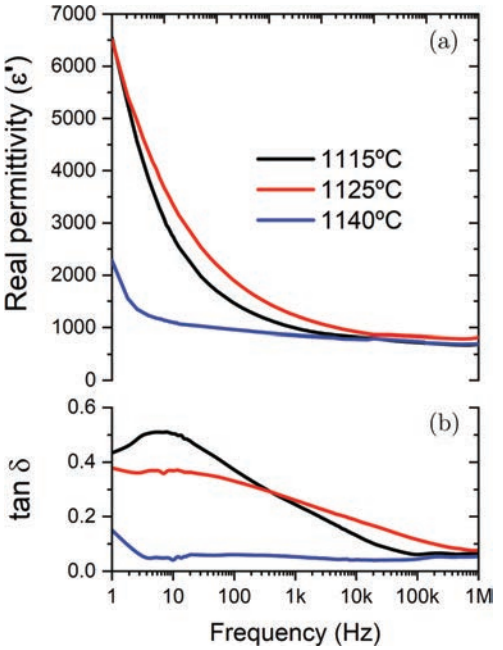

Fig. 6. Real permittivity (a) and loss tangent (tanδ) (b) at RT as a function of frequency for KNL–NTS sintered at 1115 °C, 1125 °C, and 1140 °C.

degree (~95%). For all the samples, the high-density registered values allow the dielectric, ferroelectric, and piezoelectric properties evaluation and the possible correlation between final properties and the selected sintering temperature.

Real permittivity and dielectric losses as a function of frequency are shown in Fig. 6. It can be observed that dielectric properties are similar to those reported by other researchers.[18,25] However, ceramics obtained at the highest sintering temperature (1140 °C) present the lowest real permittivity values in the studied frequency range. This effect could be associated with the preferential stabilization of the orthorhombic perovskite structure, the highest medium grain size, and the notable secondary phase formation favored by the alkaline elements' volatilization. Besides, the dielectric permittivity (ε') decreases rapidly with the increase in frequency. This diminution could be related to a space charge relaxation process. The sample sintered at 1140 °C presents low real permittivity values, as mentioned before, and low dielectric loss values. However, dielectric losses increase as the frequency values decrease. This response in frequency could be associated to the space charges polarization.

Figure 7 displays the temperature dependence of the real permittivity ε' (at 500 kHz) of KNL–NTS ceramics sintered at 1125 °C, 1125 °C, and 1140 °C. In the sintered samples, two transition peaks with temperature can be observed. The first one, near 50 °C, is associated with the orthorhombic–tetragonal phase transition (T_{o-t}),[28] while the second peak, close to 300 °C, is associated with tetragonal to cubic phase transition (T_C). Considering the XRD patterns and

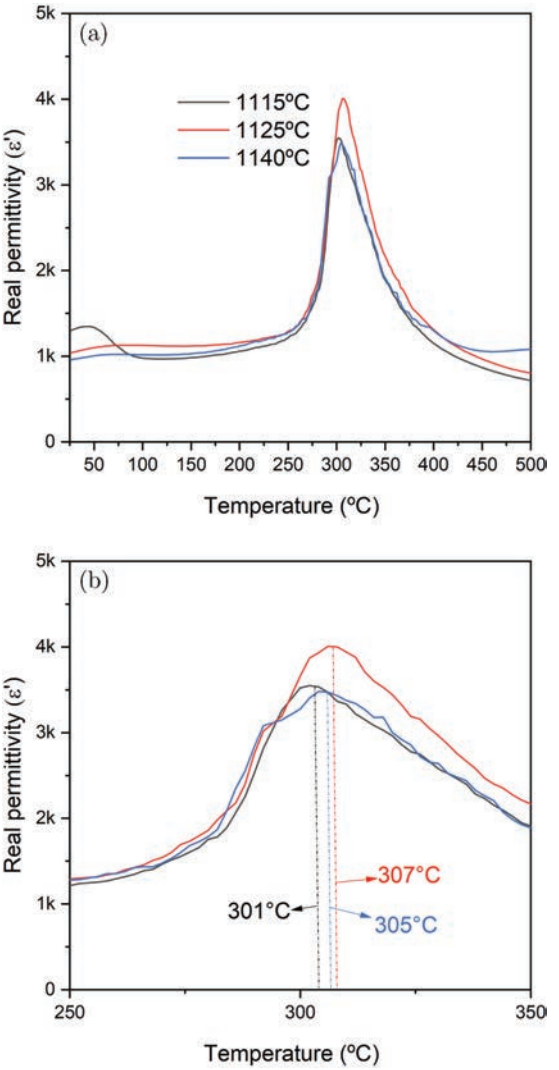

Fig. 7. (a) Real permittivity (ε') as a function of temperature of KNL–NTS specimens sintered at different temperatures (at 500 kHz). (b) Enlargement of (a) between 250 °C and 350 °C.

real permittivity curves (see Table 1 and Fig. 7), we can deduce that although all the samples show the coexistence of the orthorhombic (O) and tetragonal (T) phases, the phase equilibrium is displaced towards the orthorhombic phase. It is known that, in KNL–NTS ceramics, Li^+ stabilizes the tetragonal symmetry, and consequently, the T_{o-t} moves to lower values.[25] Consequently, the T_{o-t} displacement to higher temperatures can be attributed to the secondary phase formation that partially retains the alkaline elements (potassium and lithium). Additionally, for samples sintered at 1125 °C, the diminution in the secondary phase amount increases the tetragonal phase stability and the small increment in the Curie temperature.

Sintered samples were analyzed under an external strong electric field, exhibiting ferroelectric behavior due to the spontaneous polarization in all cases. The polarization hysteresis

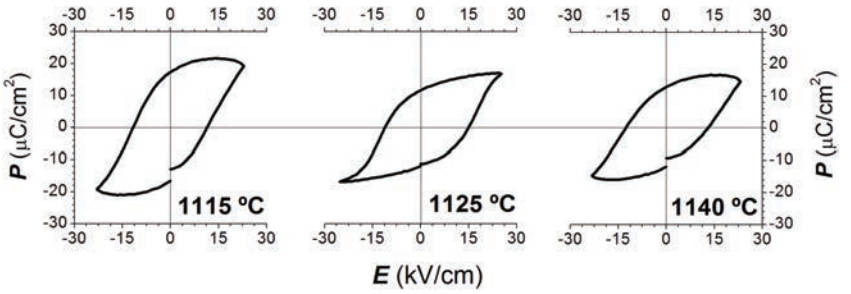

(a)

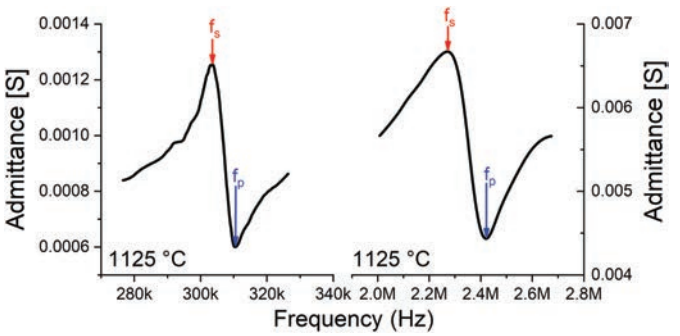

(b)

Fig. 8. (a) Hysteresis loops at room temperature of KNL–NTS sintered ceramics and (b) admittance spectra of KNL–NTS disk sintered at 1125 °C for 2 h.

loops of KNL–NTS ceramics at room temperature and under different electric fields (up to E_p = 30 kV/cm) are shown in Fig. 8(a). Samples sintered at 1115 °C and 1140 °C displayed rounded hysteresis loops whereas in samples sintered at 1125 °C hysteresis loops were not completely saturated. Ceramics sintered at 1115 °C and 1140 °C show remnant polarization (P_r) close to 17.3 μC/cm^2 and 13.0 μC/cm^2, higher than the value measured in the sample obtained at 1125 °C (~11.63 μC/cm^2). The registered coercive fields were 11.42, 15.03, and 12.95 kV/cm for the samples sintered at 1115 °C, 1125 °C, and 1140 °C, respectively. To explain the observed loops, possible alternatives were evaluated. Taking into account that all samples registered similar density values, the observed changes in the hysteresis loops cannot be attributed to the porosity fluctuations. On the other hand, the volatilization of alkaline elements also produces vacancies in the perovskite A-site, facilitating the movement of the ferroelectric domains and the polarization switching, and, subsequently, softening the hysteresis loops with the increasing sintering temperature. Moreover, the influence of the KNL–NTS grain size on the domains movement apparently is not relevant, because the grain size practically does not change for samples sintered at 1115 °C or 1125 °C, whereas important changes in the hysteresis loops are observed. Here, the secondary phase contribution must be considered as a relevant modifier of the hysteresis loops. It was reported the existence of ionic conduction in $K_3LiNb_6O_{17}$ attributed to the Lithium movement in the solid solution. In this tungsten-bronze-like structure, about 53% of the Li-sites are vacant. Consequently, Li ions in these materials are expected to move over the materials through the vacant sites.[29] Therefore, the observed changes in the hysteresis loops can be attributed to variations in both the secondary phase amount and distribution throughout the sample, as well as, inhomogeneities in the A- and B-sites of the principal phase generated during the secondary phase formation. In addition, changes in the orthorhombic/tetragonal stabilized structure also produce changes in the polarization. Indeed, Rubio-Marcos and colleagues determined that the best piezoelectric properties and, consequently, spontaneous polarizations are obtained for the tetragonal symmetry for $(KNL)_{1-x}Mn_{x/2}$–NTS ceramics depending on the MnO content.[25]

Table 3 shows the piezoelectric constant (d_{33}), and coupling factors (K_p and K_t) of sintered samples at different temperatures. It can be observed that ceramics samples sintered at 1125 °C register the best piezoelectric properties due to a balance between the stabilized perovskite structure around the MPB, the densification degree, the alkaline elements volatilization, and the amount of the secondary phase. The further increase of the sintering temperature leads to obvious decreases in d_{33} and K_p which are partly caused by the volatilization of Na and K during high-temperature sintering.

Finally, Fig. 8(b) shows the admittance spectra of KNL–NTS disk sintered at 1125 °C for 2 h. The f_s and f_p frequencies are visible in the 280 to 340 kHz and 2.0 to 2.8 MHz range; the highest values of d_{33}, $K_{p,}$ and K_t are obtained in ceramics

sintered at 1125 °C. At this sintering temperature, the conjunction between the secondary phase amount, the stabilized perovskite structure, the grain size, and the densification degree, favors the reversible polarization.

4. Conclusion

Microstructure, phase transition, and electric properties of KNL–NTS systems obtained by the solid-state reaction route and sintered at different temperatures have been reported. X-ray diffraction patterns showed the formation of KNL–NTS with the perovskite-type structure where the orthorhombic/tetragonal ratio was sensitive to the sintering temperature. Additionally, the formation of a secondary phase ($K_3LiNb_6O_{17}$, KLNO) was also detected. This secondary phase retains part of the alkaline elements and displaces the orthorhombic/tetragonal ratio towards the orthorhombic phase. Microstructure morphology, secondary phase amount, and density values were modified by the sintering temperature. Samples sintered at 1125 °C showed the highest piezoelectric properties. In opposition, samples sintered at the lowest or highest temperatures registered lower properties due to the increase in the secondary phase amount, and the volatilization of alkaline elements for the highest temperatures. In conclusion, our results demonstrate that sintering conditions play a relevant role in the tuning and optimization of the functional properties of the KNL–NTS systems. Moreover, the amount of the KLNO secondary phase strongly affects the functional properties of these piezoceramics.

Acknowledgments

The authors are grateful to the National Council for Scientific and Technological Development (CNPq) and the Coordination for the Improvement of Higher Education Personnel (CAPES) for the financial support granted during this research. The authors are grateful to CONICET, ANPCyT, University of Mar del Plata (Argentina), and to the MINECO (Spain) project MAT2017-86450-C4-1-R for the financial support provided for this research.

References

[1]S. Li, A. S. Bhalla, R. E. Newnham and L. E. Cross, Quantitative evaluation of extrinsic contribution to piezoelectric coefficient d_{33} in ferroelectric PZT ceramics, *Mater. Lett.* **17**, 21 (1993).

[2]H. L. Li, Y. Zhang, J. J. Zhou, X. W. Zhang, H. Liu, and J. Z. Fang, Phase structure and electrical properties of *x*PZN-(1–*x*)PZT piezoceramics near the tetragonal/rhombohedral phase boundary, *Ceram. Int*. **41**, 4822 (2015).

[3]M. Villegas, C. Moure, J. R. Jurado and P. Duŕan, Influence of the calcining temperature on the sintering and properties of PZT ceramics, *J. Mater. Sci*. **28**, 3482 (1993).

[4]L. Zhang, Y. Pu, M. Chen, T. Wei and X. Peng, Novel $Na_{0.5}Bi_{0.5}Ti_{0.5}O_3$ based, lead-free energy storage ceramics with high power and energy density and excellent high-temperature stability, *Chem. Eng. J*. **383**, 123154 (2019).

[5]C. K. Jeong, K. I. Park, J. Ryu, G. T. Hwang and K. J. Lee, Large-area and flexible lead-free nanocomposite generator using alkaline niobate particles and metal nanorod filler, *Adv. Funct. Mater.* **24**, 2620 (2014).

[6]E. Meyer, D. Mutukwa, N. Zingwe and R. Taziwa, Lead-free halide double perovskites: A review of the structural, optical, and stability properties halide perovskites, *Metals* **8**, 667 (2018).

[7]H. Palneedi, V. Annapureddy, S. Priya and J. Ryu, Status and perspectives of multiferroic magnetoelectric composite materials and applications, *Actuators* **5**, 9 (2016).

[8]J. D. Bobić, M. M. Vijatović Petrović and B. D. Stojanović, *Metal Oxides, Magnetic, Ferroelectric, and Multiferroic Metal Oxides*, ed. B. D. Stojanović, Chapter 11 (Elsevier, 2018), pp. 233–249.

[9]R. C. Haislmaier, Y. Lu, J. Lapano, H. Zhou, N. Alem, S. B. Sinnott, R. Engel-Herbert and V. Gopalan, Large tetragonality and room temperature ferroelectricity in compressively strained $CaTiO_3$ thin films, *APL Mater*. **7**, 051104 (2019).

[10]C. Pithan, Y. Shiratori, J. Dornseiffer, F. H. Haegel, A. Magrez and R. Waser, Microemulsion mediated synthesis of nanocrystalline $(K_xNa_{1-x})NbO_3$ powders, *J. Cryst. Growth* **280**, 191 (2005).

[11]A. Chowdhury, J. Bould, Y. Zhang, C. James and S. J. Milne, Nano-powders of $Na_{0.5}K_{0.5}NbO_3$ made by a sol-gel method, *J. Nanopart. Res*. **12**, 209 (2010).

[12]J. Hao, Z. Xu, R. Chu, Y. Zhang, Q. Chen, P. Fu, W. Li. G. Li and Q. Yin, Characterization of $(K_{0.5}Na_{0.5})NbO_3$ powders and ceramics prepared by a novel hybrid method of sol–gel and ultrasonic atomization, *Mater. Des.* **31**, 3146 (2010).

[13]S. Roy, B. Biswas and S. B. Majumder, Investigations on flexible multiferroic composites, *AIP Conf. Proc.*, Vol. 1063 (2008), pp. 276–289.

[14]J. Jin, S. G. Lu, C. Chanthad, Q. Zhang, M. A. Haque and Q. Wang, Multiferroic polymer composites with greatly enhanced magnetoelectric effect under a low magnetic bias, *Adv. Mater*. **23**, 3853 (2011).

[15]R. Xiang and J. Wu, Contribution of $Bi_{0.5}Na_{0.5}ZrO_3$ on phase boundary and piezoelectricity in $K_{0.48}Na_{0.52}Nb_{0.96}Sb_{0.04}O_3$-$Bi_{0.5}Na_{0.5}SnO_3$-*x*$Bi_{0.5}Na_{0.5}ZrO_3$ ternary ceramics, *J. Alloys Compd*. **684**, 397 (2016).

[16]X. Tang, T. Chen, Y. Liu, J. Zhang, T. Zhang, G. Wang and J. Zhou, Composition dependence of phase structure and electrical properties in (0.98-*x*)$K_{0.35}Na_{0.65}NbO_3$–0.02$BaZrO_3$–*x*$Bi_{0.5}Na_{0.5}ZrO_3$ ternary ceramics, *J. Alloys Compd*. **672**, 277 (2016).

[17]F. Z. Yao, Q. Yu, K. Wang, Q. Li and J. F. Li, Ferroelectric domain morphology and temperature-dependent piezoelectricity of (K,Na,Li)(Nb,Ta,Sb)O_3 lead-free piezoceramics, *RSC Adv*. **4**, 20062 (2014).

[18]L. Ramajo, M. Castro, A. del Campo, J. F. F. Fernandez and F. Rubio-Marcos, Influence of B-site compositional homogeneity on properties of $(K_{0.44}Na_{0.52}Li_{0.04})(Nb_{0.86}Ta_{0.10}Sb_{0.04})O_3$-based piezoelectric ceramics, *J. Eur. Ceram. Soc*. **34**, 2249 (2014).

[19]X. Yan, B. Peng, X. Lu, Q. Dong and W. Li, Structure evolution and enhanced piezoelectric properties of $(K_{0.5}Na_{0.5})NbO_3$-0.06$LiTaO_3$-$SrZrO_3$ lead-free ceramics, *J. Alloys Compd.* **653**, 523 (2015).

[20]R. N. Nandini, M. Krishna, A. V. Suresh and K. Narasimha Rao, Effect of calcination kinetics and microwave sintering parameters on dielectric and peizo-electric properties of $(K_{0.5}Na_{0.5})NbO_3$ ceramics, *Iran. J. Mater. Sci. Eng*. **15**, 14 (2018).

[21]Y. Saito, H. Takao, T. Tani, T. Nonoyama, K. Takatori, T. Homma, T. Nakamura and N. Masaya, Lead-free piezoceramics, *Nature* **432**, 81 (2004).

[22]F. Rubio-Marcos, J. J. Romero and J. F. Fernandez, Effect of the temperature on the synthesis of (K,Na)NbO_3-modified nanoparticles by a solid state reaction route, *J. Nanopart. Res*. **12**, 2495 (2010).

[23]T. Zheng, J. Wu, D. Xiao and J. Zhu, Recent development in lead-free perovskite piezoelectric bulk materials, *Prog. Mater. Sci*. **98**, 552 (2018).

[24]Y. Chen, S. Wang, H. Zhou, G. Xu, Q. Wang and J. Zhu, A systematic analysis of the radial resonance frequency spectra of the PZT-based (Zr/Ti = 52/48) piezoceramic thin disks. *J. Adv. Ceram.* **9**, 380 (2020).

[25]F. Rubio-Marcos, P. Marchet, X. Vendrell, J. J. Romero, F. Rémondière, L. Mestres and J.F. Fernández, Effect of MnO doping on the structure, microstructure and electrical properties of the (K,Na,Li)(Nb,Ta,Sb)O_3 lead-free piezoceramics, *J. Alloys Compd*. **509**, 8804 (2011).

[26]J. Ravez and A. Simon, Some solid state chemistry aspects of lead-free relaxor ferroelectrics, *J. Solid State Chem*. **162**, 260 (2001).

[27]Y. Wang, D. Damjanovic, N. Klein and N. Setter, High-temperature instability of Li- and Ta-modified (K,Na)NbO_3 piezoceramics, *J. Am. Ceram. Soc.* **91**, 1962 (2008).

[28]F. Rubio-Marcos, P. Marchet, J. R. Duclère, J. J. Romero and J. F. Fernández, Evolution of structural and electrical properties of (K,Na,Li)(Nb,Ta,Sb)O_3 lead-free piezoceramics through CoO doping, *Solid State Commun*. **151**, 1463 (2011).

[29]J. Tanaka, M. Tsukioka, E. Bannai, M. Shimazu and S. Ehara, 1982). Ionic conduction in $K_3LiNb_6O_{17}$ and $K_3LiTa_6O_{17}$, *J. Mater. Sci. Lett*. **1**, 133 (1982).